

## Deep UV sensing of the interaction of porphyrin with bovine serum albumin protein

— [Source link](#) 

Qiang Li, Stefan Seeger



**Institutions:** University of Zurich

**Published on:** 20 May 2009 - Sensors and Actuators B-chemical (Elsevier)

**Topics:** Fluorescence spectroscopy, Fluorescence cross-correlation spectroscopy, Laser-induced fluorescence, Fluorescence in the life sciences and Resonance fluorescence

Related papers:

- [Principles of fluorescence spectroscopy](#)
- [Changes in porphyrin nonlinear absorption owing to interaction with bovine serum albumin.](#)
- [Spectroscopic studies on the interaction of colloidal capped CdS nanoparticles with bovine serum albumin.](#)
- [New water-soluble dicyano-stilbene dyes: One and two-photon fluorescence and photo-response to BSA](#)
- [Absorption and Fluorescence Studies of 3-Ethenylindoles](#)

Share this paper:    

View more about this paper here: <https://typeset.io/papers/deep-uv-sensing-of-the-interaction-of-porphyrin-with-bovine-1eou0jlqjn>



University of Zurich  
Zurich Open Repository and Archive

Winterthurerstr. 190  
CH-8057 Zurich  
<http://www.zora.uzh.ch>

---

*Year: 2009*

---

## Deep UV sensing of the interaction of porphyrin with bovine serum albumin protein

Li, Q; Seeger, S

Li, Q; Seeger, S (2009). Deep UV sensing of the interaction of porphyrin with bovine serum albumin protein. *Sensors and Actuators B: Chemical*, 139(1):118-124.

Postprint available at:  
<http://www.zora.uzh.ch>

Posted at the Zurich Open Repository and Archive, University of Zurich.  
<http://www.zora.uzh.ch>

Originally published at:  
*Sensors and Actuators B: Chemical* 2009, 139(1):118-124.

# Deep UV sensing of the interaction of porphyrin with bovine serum albumin protein

## Abstract

The interaction of meso-tetrakis(p-sulfonatophenyl)porphyrin (TPPS) with bovine serum albumin (BSA) in neutral solution (pH 7.4) has been studied by means of absorption, steady-state fluorescence and time-resolved fluorescence spectroscopy. The formation of TPPS-BSA complex was monitored by spectroscopic characteristic changes in Soret band absorption and fluorescence emission of TPPS. Applying the time-correlated single-photon counting (TCSPC) method, BSA-TPPS interaction was also investigated by the fluorescence lifetime of tryptophan residues in BSA. The results demonstrate that deep UV laser-based fluorescence lifetime microscopy is useful for sensitive identification of protein interaction using intrinsic fluorescence.

# **Deep UV sensing of the interaction of porphyrin with bovine serum albumin protein**

Qiang Li and Stefan Seeger <sup>a</sup>

*Institute of Physical Chemistry, University of Zurich,  
Winterthurerstrasse 190, CH-8057 Zurich, Switzerland*

## **Abstract**

The interaction of meso-tetrakis(p-sulfonatophenyl)porphyrin (TPPS) with bovine serum albumin (BSA) in neutral solution (pH 7.4) has been studied by means of absorption, steady-state fluorescence and time-resolved fluorescence spectroscopy. The formation of TPPS-BSA complex was monitored by spectroscopic characteristic changes in Soret band absorption and fluorescence emission of TPPS. Applying the time-correlated single-photon counting (TCSPC) method, BSA-TPPS interaction was also investigated by the fluorescence lifetime of tryptophan residues in BSA. The results demonstrate that deep UV laser-based fluorescence lifetime microscopy is useful for sensitive identification of protein interaction using intrinsic fluorescence.

*Keywords:* Water soluble porphyrin; Bovine Serum Albumin; Time resolved fluorescence; Intrinsic fluorescence

---

<sup>a</sup> Author to whom correspondence should be addressed:  
Fax: +41- 44 -6356813  
E-mail: sseeger@pci.uzh.ch (S. Seeger)

## 1. Introduction

Photodynamic therapy is one of the most promising new agents for the treatment of cancers, in which light-activated sensitizers are used to selectively destroy abnormal tissues [1, 2]. In recent years there has been a growing interest in the use of porphyrins and related compounds as therapeutic drugs. They are applied in medicine on important areas as cancer detection and photosensitizers in photodynamic therapy of cancer [3-6]. Potential applications of porphyrins have recently appeared in the treatment of nonmalignant conditions such as psoriasis, atheromatous plaque, viral and bacterial infections including HIV [7, 8], and blood substitutes [9].

Meso-tetrakis(p-sulfonatophenyl)porphyrin (TPPS) is a water soluble porphyrin. In neutral solutions TPPS exists in deprotonated form possessing negative charges on four sulfonic residuals. When the acidity and/or ionic strength increases ( $\text{pH} < 4.8$ ), two protons bind to central nitrogen atoms inducing partial positive charge in the center of the porphyrin ring. At even higher acidity ( $\text{pH} < 2$ ), additional protons can bind to  $\text{SO}_3^-$  groups and shield their negative charge. J-aggregates are formed via electrostatic interaction between positively charged porphyrin center and negatively charged  $\text{SO}_3^-$  groups of neighboring TPPS. The J-aggregation of TPPS at low pH and/or high ionic strength has been studied extensively. The structure, aggregation number, absorption spectra, quantum yield and excited state of TPPS J-aggregates in acidic aqueous solution have been reported so far [10-18].

Deprotonated and protonated monomeric forms of TPPS have different absorption and fluorescence spectra [19, 20] (Table 1), At pH 7, the absorption spectra of deprotonated species exhibits features of  $D_{2h}$  symmetry with Soret band at 413 nm and Q-band at 516, 553, 579, 633 nm. However, at high acidity symmetry of the protonated increases to  $D_{4h}$

featuring a shift of the Soret band from 413 to 434 nm and the nonsplitting of the Q-bands (594 and 645 nm). Two new absorption bands, a sharp excitonic band at ~ 490 nm and the second one at ~ 705 nm, appear simultaneously by increasing the acidity ( $\text{pH} < 2$ ). These two new bands have been assigned to the formation of J-aggregates of TPPS protonated form. The narrowed absorption band observed for J-aggregates is due to the coherent delocalization of excitations over an aggregate caused by the intermolecular interaction between transition dipole moments of TPPS molecules [21]. The formation of TPPS J-aggregates was reported occurring not only in pure aqueous medium but also in mixed solutions such as surfactants [22-25], proteins [19, 20, 26-29], polypeptides [30, 31], and cyclodextrins [32] at higher acidity ( $\text{pH} < 2$ ).

Bovine Serum Albumin (BSA), also known as "Fraction V", is a very interesting molecule in terms of biochemistry and biophysics and has been studied intensively over the last few decades. It is the major protein species found in bovine blood plasma and has applications in life science disciplines such as cell culture, in-vitro diagnostics, human and veterinary pharmaceuticals, molecular biology, serology and general research. In restriction digests, BSA is used to stabilize some enzymes during digestion of DNA and to prevent adhesion of the enzyme to reaction tubes and other vessels [33]. The primary structure of BSA is very well known consisting of 583 amino acid residues, whereas its secondary structure contains 67% of alpha helix and 17 disulfide bridges that confer to the protein a remarkable stability [33, 34]. BSA displays native fluorescence when excited in the UV region of 260 to 280 nm [35], it contains two tryptophan residues which are located at positions 134 and 213 of the chain.

Ultrasensitive protein detection can be achieved by using highly efficient fluorescence labels. However, the labeling procedure is usually time consuming and expensive, the introduction of fluorophores may change the proteins physical properties, such as

charge, hydrophobic/hydrophilic character and structure. In order to avoid these disadvantages, direct ultrasensitive measurements of native fluorescence of proteins have been developed [36-39]. Recently we could show for the first time the single molecule and single protein detection without any labeling using deep UV laser-based fluorescence lifetime microscopy [40-42]. This method is also quite useful for sensitive identification of protein interactions and for direct analysis of protein in one-dimensional separation coupled with miniaturized PAA gel electrophoresis [43, 44].

The photobiological activity of porphyrin depends on its physico-chemical properties. Activation of the porphyrin photosensitizer leads to the formation of porphyrin triplet states and singlet oxygen, the main cell killer in photodynamic therapy. The water soluble porphyrin of TPPS exhibits a high quantum yield of singlet oxygen, equal to 0.62 in water [32]. In clinical application, the approach that utilizes pre-association of a sensitizer with endogenous carriers such as serum albumin in blood followed by dissociation of the complex inside the cell during the metabolic processes seems to be particularly appealing. Porphyrins are usually introduced in the blood as relatively concentrated solution, which may diminish its action or even cause adverse effects. For instance, the formation of protein complexes reduces the quantum yield of singlet oxygen photogenerated by TPPS, which changes the photobiological activity of TPPS [45]. Hence, deep understanding of interaction between TPPS and protein in different acidity solution is crucial for further progress in photodynamic therapy of tumours.

The influence of proteins on the formation of J-aggregates of TPPS in aqueous acid solution ( $\text{pH} < 2$ ) has been investigated [19, 20, 26-29]. In the present work, we aim to investigate the interaction of TPPS with BSA in physiological environment ( $\text{pH} 7.4$ ). The binding characteristics were studied by absorption, steady-state and time-resolved deep UV fluorescence spectroscopy. A global analysis fitting revealed the formation of

BSA-TPPS complex in PBS buffer solution (pH 7.4). The mean fluorescence lifetime between BSA and TPPS bound BSA decreases dramatically, which can be used for sensitivity detection of BSA-TPPS interaction.

## **2. Experimental**

### *2.1 Materials*

The pure BSA and N-Acetyl-L-tryptophanamide (NATA) were purchased from Sigma and TPPS was obtained from Fluka. BSA was solved and diluted in phosphate buffered saline solution (PBS, pH 7.4), NATA and TPPS were solved and diluted in double distilled water. All other chemicals were of analytical grade.

### *2.2 Sample preparation*

For absorption and steady-state fluorescence experiments TPPS concentration was kept constant at 2  $\mu\text{M}$ , while BSA concentration was varied to reach TPSS:BSA molar ratios from 1:0.01 to 1:20. Absorption spectra of solutions were measured with UV/VIS/NIR-spectroscopy Lambda 900 (Perkin Elmer). Steady-state fluorescence spectra were obtained in standard quartz cuvettes with a luminescence spectrometer LB 50B (Perkin Elmer) equipped with a red-sensitive photomultiplier tube (Hamamatsu R-928). Time-resolved fluorescence spectroscopy of BSA and BSA-TPPS complex solutions were measured with home-made UV Fluorescence Lifetime Microscopy by putting 100  $\mu\text{l}$  sample on quartz cover slides which glued to aluminum slabs with six reaction vessels containing a volumetric capacity of 300  $\mu\text{l}$ . The experiments have been performed at a constant BSA concentration of 1  $\mu\text{M}$  and TPPS concentration was varied. Prior to use the quartz cover slides (SPI Supplies, 170  $\mu\text{m}$  thickness) were cleaned for 60 min in



CHCl<sub>3</sub> in an ultrasonic bath followed by washing with double distilled water and then dried in nitrogen flow. The fluorescence of NATA shows a single-exponential decay with lifetime of  $2.85 \pm 0.05$  ns [46], which was used as standard to calibrate the instrument response. For the data analysis commercial software FluoFit by PicoQuant was used. The experimental data were analyzed using Marquardt-Levenberg algorithm. The decay parameters were determined by least-squares deconvolution using multi-exponential models, and their quality was judged by the reduced  $\chi^2$  value and the randomness of the weighted residuals. All experiments were done at room temperature.

### *2.3 UV Fluorescence Lifetime Microscopy.*

The time-resolved fluorescence studies were carried out with UV fluorescence lifetime microscopy described elsewhere[40, 41]. It consists of a 266 nm UV mode-locked diode-pumped picosecond laser (GE-100-XHP-FHG, Time-Bandwidth Products Inc., Switzerland). The laser system provides pulses with a duration of less than 10 ps and with a repetition rate of 40 MHz, maximum output power is 20 mW. The polarized laser beam was split 50/50 by a beam splitter (Laser components GmbH, Germany) sending 50% into a high speed photodiode module (PHD-400, Becker & Hickl GmbH, Berlin, Germany) which is used as deriving the synchronization signal for triggering of the time-correlated single photon counting module. The second beam passed an excitation filter (254WB25, Omega Optical) and is directed into the quartz microscope objective (40 $\times$ , NA = 0.80, Partec GmbH, Münster, Germany) by a dichroic beamsplitter (290DCLP, Omega Optical). The laser power was adjusted by inserting different neutral density filters (Melles Griot). An automatic beam shutter is incorporated to minimize the unnecessary exposure time which prevented the protein from bleaching. The fluorescence light was collected by the same objective and transmitted through the dichroic mirror. An achromatic lens (LAU-25-200, OFR Inc., 200 mm focal distance)

focuses the light onto a pinhole. After the pinhole, the fluorescence emission is detected by a high speed photomultiplier tube (PMT) detector head (PMH-100-6, Becker & Hickl GmbH, Berlin, Germany). Two emission bandpass filters (330WB60, Omega Optical), one positioned directly after the lens, the other directly in front of the detector, discriminate fluorescence against scattered light. The signal pulses of the PMT was fed into a time-correlated single-photon counting (TCSPC) PC interface card (SPC-630, Becker & Hickl GmbH, Berlin, Germany) to acquire time-resolved data. The time-correlated single-photon counting was performed in the reversed mode, i.e. the signal of the PMT was used to start the clock of the time-to-amplitude converter and the reference signal of the laser from high speed photodiode was used as stop signal. The instrument response function (IRF) was measured by replacing the sample with a scattering dispersion of colloidal silicon dioxide particles in water (particle size 11 nm), and then recording the Rayleigh scattering of the excitation light without two emission filters. With this setup an IRF of 240 ps (FWHM) was measured. The fluorescence decay time constants were obtained by deconvoluting the instrument response function.

### **3. Results and discussion**

The absorption spectra of TPPS in PBS solution and in the presence of different concentration of BSA at pH 7.4 are shown in Figure 1. As was shown earlier [19, 20], in the absence of BSA the absorption spectra consisted of Soret band at 413 nm and Q-band at 516, 552, 579, 635 nm, which belong to a deprotonated monomeric form TPPS. Titrations of TPPS solutions at a fixed TPPS concentration (2  $\mu$ M) and varying BSA were performed in PBS buffer solution at pH 7.4. The addition of BSA changes position, width, and intensity of the bands in absorption spectra of TPPS. The intensity of Soret band decreased in the presence of BSA at small ratios (TPPS:BSA, 1:0.1 to

1:0.3). With the decreased intensity a slight red shift of Soret band and the broadening of its red side were observed (insert Figure 1). With continued increase of BSA concentration in mixed solutions (TPPS:BSA, 1:0.5 to 1:20), the absorbance of Soret band increases and reaches its maximum values within TPPS:BSA molar ratios range from 1:10 to 1:20 together with a red shift of this band from 413 to 422 nm. The similar changes in Q-bands were obtained with increase of BSA concentration, the maxima of those bands shifted to 518, 553, 593, and 648 nm when molar ratio of TPPS:BSA = 1:20. Protonated monomeric and J-aggregated forms of TPPS have not been observed in the PBS solution at pH 7.4.

Using absorption spectra, it is possible to decompose TPPS Soret band in a sum of three Gaussian functions indicated as dot-dashed, dotted and dashed lines in Figure 2. The left component (dot-dashed line) centered at ~405 nm almost keeps the same absorption intensity in the absence and presence of different concentration of BSA, which is the shoulder of the Soret band absorption. The middle and right component (dotted and dashed lines) have maximum absorption at 413 and 422 nm, respectively. The increase of BSA concentration reduces the contribution of the middle component, the absorption intensity becomes zero when the molar ratio of TPPS:BSA is 1:20. Thus, the middle component can be assigned to free TPPS. However, the contribution of the right component increases when the concentration of BSA increases, the absorption intensity of this component reaches maximum at TPPS:BSA = 1:20. We can ascribe this component to BSA bound TPPS form. The absorption intensity of the middle and right components plotted versus the BSA protein concentration shows the growth of the bound TPPS forms and the decrease of the free TPPS forms (Figure 3). The Q bands which located at 510-650 nm are not fitted due to weak absorbance compared to the Soret band.

Figure 3 shows a nonlinear relationship between the absorbance of bound TPPS and the amount of BSA added, which indicates either that there is more than one class of binding sites or that the binding of each successive molecule alters the association constant of the next molecule. A similar behavior has been observed for binding of TPPS with human serum albumin (HSA) [20]. The value of binding constant  $K$  is quite high at all pHs, which indicates important electrostatic interactions in the TPPS-HAS complex. We use same equation (Eq. 1 in Ref. 20) to determine the binding parameters, the value of  $n$  is  $1.2 \pm 0.3$  with the binding constant  $K$  of  $(4.5 \pm 0.9) \times 10^6 \text{ M}^{-1}$ .

Two excitation wavelengths were chosen for recording the fluorescence emission spectra since the absorption peak changes observed in the absence and presence of BSA solution. The fluorescence emission spectra for the different molar ratios of TPPS:BSA at excitation wavelength 413 and 422 nm are shown in Figure 4, respectively. Under both excitation wavelengths, the fluorescence spectra for the free TPPS form manifested a single fluorescence band with a peak at 639 nm. Increasing the molar ratio of TPPS:BSA (from 1:0.1 to 1:50), the fluorescence emission peak shifted to longer wavelengths and finally is located at 648 nm. The fluorescence emission spectra kept unchanged within TPPS:BSA molar ratios range from 1:10 to 1:20, we can assign these fluorescence spectra to the BSA bound TPPS form. However, the fluorescence emission intensity shows different characteristic. The intensity decreases at 413 nm excitation and increases at 422 nm excitation when the concentration of BAS solution increases, which in accordance with absorption data because of decreasing of the free TPPS form and increasing of the BSA bound TPPS form in the titration procedure.

The fluorescence spectra of this titration procedure also can be decomposed to two Gaussian distributions as shown in Figure 5 for TPPS:BSA molar ratio of 1:0.5 at excitation wavelength of 413 and 422 nm, respectively. The left component (dotted line)

has its maximum emission at 639 nm. The contribution of this component decreases with increasing BSA concentration (insert Figure 4), the emission intensity becomes zero when the molar ratio of TPPS:BSA is 1:20. Thus, the left component can be assigned to the fluorescence emission of free TPPS. However, the contribution of the right component (centered at 648 nm) increases with increasing of BSA molar ratios (insert Figure 4), the emission intensity of this component reaches its maximum at high TPPS concentration. We can ascribe this component to the fluorescence emission of BSA bound TPPS form.

Andrade and coworkers [20] investigated the fluorescence decay of TPPS in the presence of human serum albumin (HSA) protein at pH 7 upon excitation at 425 nm and emission at 650 nm, a global analysis fitting shows two lifetime components at 9.8 and 12.9 ns. They assigned the shorter lifetime component to deprotonated free TPPS and the long-lived component to the HSA-TPPS complex. Our deep UV fluorescence lifetime microscopy has a fixed excitation wavelength at 266 nm, i.e. we have had to measure BSA as a probe, because TPPS excitation wavelength doesn't match with the emission of our setup. Upon excitation at 266 nm, BSA displays an intrinsic fluorescence emission band around 340 nm mainly due to tryptophan residues. The fluorescence decay characterization of BSA in absence and presence of TPPS in PBS buffer solution at pH 7.4 is shown in Figure 6. The lifetime, relative amplitudes and  $\chi^2$  of the decay of BSA-TPPS system obtained by global analysis with three-exponential fit are listed in Table 2. Figure 7(a) shows the fluorescence decay of pure BSA in PBS buffer solution to together with the IRF of our instrument. The decay is of single-exponential type with lifetime of 5.21 ns. The fluorescence decay of BSA in presence of TPPS with molar ratio of BSA:TPPS = 1:3 is shown in Figure 7(b). The analysis of the fluorescence decay data show three components with different decay times 5.21, 3.86, and 0.55 ns.

The long lifetime component can be assigned to free BSA in the mixture because it has the same lifetime as pure BSA solution without added TPPS. The medium and short lifetime components have been obtained with keeping BSA at constant concentration (1 $\mu$ M) and varying the TPPS concentration, these two components can be assigned to the TPPS bound BSA species. When BSA:TPPS molar ratio reach the value 1:20, the fluorescence decay shows only two components (3.86 and 0.55 ns) and the amplitude of the long lifetime ( $\tau_1 = 5.21$  ns) component comes close to zero (Figure 7(c)). The equilibrium constant of BSA and TPPS interaction is  $(5.0 \pm 1.8) \times 10^6 \text{ M}^{-1}$  [26, 47], the amount of TPPS was sufficient to ensure total BSA binding to TPPS at this molar ratio. The insert of Figure 6 shows the amplitude changes of each lifetime in this titration process. The fluorescence lifetime distribution of free BSA and TPPS bound BSA indicates a conformation change of BSA induced by TPPS. The tryptophan residues are located in a different microenvironment before and after binding to TPPS.

The mean fluorescence lifetime of BSA and TPPS bound BSA is 5.21 and 2.71 ns, respectively. This decrease in the mean lifetime was used to quantify the sensitivity of our method for the BSA-TPPS interaction. The mean fluorescence lifetime changes between free BSA and the BSA-TPPS complex measured by keeping the molar ratio of BSA:TPPS at 1:20 and varying the BSA concentration. We are able to detect fluorescence lifetime changes with BSA concentrations down to nanomolar concentration range.

#### **4. Conclusion**

We investigated the spectral and kinetic manifestations of interaction BSA with TPPS in PBS buffer solution. The analysis of the absorption and fluorescence emission spectra

of TPPS shows the formation of BSA bound TPPS complex in the presence of BSA solution. The fluorescence decay of BSA in the presence of different concentration of TPPS was analyzed by reconstructing the decay time distributions with multiexponential models. The effect of binding TPPS to BSA is shown to be a decrease of the mean fluorescence lifetime from 5.21 ns to 2.71 ns, the profile of fluorescence decay change from single-exponential decay to double-exponential decay. This effect is explained by a conformation change of BSA protein induced by TPPS. With the molecular system described we have shown that ultrasensitive confocal time-resolved deep UV fluorescence microscopy is an ideal tool to study intermolecular interactions at very low concentrations. Hence, with this method high information content about molecular interactions can be generated with small sample volume and at low concentrations respectively.

### **Acknowledgements**

We thank Dr. Eugene Riaplov and Andreas Schug for helpful discussions. This work was supported by the Swiss National Science Foundation.

## References

- [1] B. W. Henderson, T. J. Dougherty, How does photodynamic therapy work? *Photochem. Photobiol.* 55 (1992) 145-157.
- [2] J. Moan, K. Berg, Photochemotherapy of cancer: experimental research, *Photochem. Photobiol.* 55 (1992) 931-948.
- [3] R. Bonnett, Photosensitizers of the porphyrin and phthalocyanine series for photodynamic therapy, *Chem. Soc. Rev.* 24 (1995) 19-33.
- [4] M. Ochsner, Photophysical and photobiological processes in the photodynamic therapy of tumors, *J. Photochem. Photobiol.*, B 39 (1997) 1-18.
- [5] R. C. Krieg, H. Messmann, K. Schlottmann, E. Endlicher, S. Seeger, J. Schoelmerich, R. Knuechel, Intracellular localization is a cofactor for the phototoxicity of protoporphyrin IX in the gastrointestinal tract: In vitro study, *Photochem. Photobiol.* 78 (2003) 393-399.
- [6] R. C. Krieg, H. Messmann, J. Rauch, S. Seeger, R. Knuechel, Metabolic characterization of tumor cell-specific protoporphyrin IX accumulation after exposure to 5-aminolevulinic acid in human colonic cells, *Photochem. Photobiol.* 76 (2002) 518-525.
- [7] E. Ben-Hur, B. Horowitz, Advances in photochemical approaches for blood sterilization, *Photochem. Photobiol.* 62 (1995) 383-388.
- [8] D. E. Lewis, R. E. Utecht, M. M. Judy, J. L. Matthews, T. C. Chanh, Photochemical neutralization of HIV-1 and inhibition of HIV-1-induced syncytium formation by halogenated 1,8-naphthalimides, *Spectrum* 6 (1993) 8-14.
- [9] J. B. Cannon, Pharmaceutics and drug delivery aspects of heme and porphyrin therapy, *J. Pharm. Sci.* 82 (1993) 435-446.
- [10] O. Ohno, Y. Kaizu, H. Kobayashi, J-aggregate formation of a water-soluble porphyrin in acidic aqueous media, *J. Chem. Phys.* 99 (1993) 4128-4139.
- [11] J. M. Ribo, J. Crusats, J. A. Farrera, M. L. Valero, Aggregation in water solutions of tetrasodium diprotonated meso-tetrakis(4-sulfonatophenyl)porphyrin, *J. Chem. Soc., Chem. Commun.* (1994) 681-682.
- [12] R. F. Pasternack, K. F. Schaefer, P. Hambright, Resonance light-scattering studies of porphyrin diacid aggregates, *Inorg. Chem.* 33 (1994) 2062-2065.



- [13] D. L. Akins, H. R. Zhu, C. Guo, Absorption and Raman scattering by aggregated meso-Tetrakis(p-sulfonatophenyl)porphine, *J. Phys. Chem.* 98 (1994) 3612-3618.
- [14] N. C. Maiti, M. Ravikanth, S. Mazumdar, N. Periasamy, Fluorescence dynamics of noncovalently linked porphyrin dimers, and aggregates, *J. Phys. Chem.* 99 (1995) 17192-17197.
- [15] P. J. Collings, E. J. Gibbs, T. E. Starr, O. Vafek, C. Yee, L. A. Pomerance, R. F. Pasternack, Resonance light scattering and Its application in determining the size, shape, and aggregation number for supramolecular assemblies of chromophores, *J. Phys. Chem. B* 103 (1999) 8474-8481.
- [16] N. Micali, F. Mallamace, A. Romeo, R. Purrello, L. M. Scolaro, Mesoscopic structure of meso-Tetrakis(4-sulfonatophenyl)porphine J-aggregates, *J. Phys. Chem. B* 104 (2000) 5897-5904.
- [17] N. Micali, A. Romeo, R. Lauceri, R. Purrello, F. Mallamace, L. M. Scolaro, Fractal structures in homo- and heteroaggregated water soluble porphyrins, *J. Phys. Chem. B* 104 (2000) 9416-9420.
- [18] A. Miura, Y. Shibata, H. Chosrowjan, N. Mataga, N. Tamai, Femtosecond fluorescence spectroscopy and near-field spectroscopy of water-soluble tetra(4-sulfonatophenyl)porphyrin and its J-aggregate, *J. Photochem. Photobiol., A* 178 (2006) 192-200.
- [19] J. Valanciunaite, S. Bagdonas, G. Streckyte, R. Rotomskis, Spectroscopic study of TPPS<sub>4</sub> nanostructures in the presence of bovine serum albumin, *Photochem. Photobiol. Sci.* 5 (2006) 381-388.
- [20] S. M. Andrade, S. M. B. Costa, Spectroscopic studies on the interaction of a water soluble porphyrin and two drug carrier proteins, *Biophys. J.* 82 (2002) 1607-1619.
- [21] H. Kano, T. Saito, T. Kobayashi, Dynamic intensity borrowing in porphyrin J-aggregates revealed by sub-5-fs spectroscopy, *J. Phys. Chem. B* 105 (2001) 413-419.
- [22] N. C. Maiti, S. Mazumdar, N. Periasamy, J- and H-aggregates of porphyrins with surfactants: fluorescence, stopped flow and electron microscopy studies, *J. Porphyr. Phthalocyanines* 2 (1998) 369-376.

- [23] N. C. Maiti, S. Mazumdar, N. Periasamy, J- and H-aggregates of porphyrin-surfactant complexes: time-resolved fluorescence and other spectroscopic studies, *J. Phys. Chem. B* 102 (1998) 1528-1538.
- [24] M. A. Castriciano, A. Romeo, V. Villari, N. Micali, L. M. Scolaro, Nanosized porphyrin J-aggregates in water/AOT/decane microemulsions, *J. Phys. Chem. B* 108 (2004) 9054-9059.
- [25] S. M. Andrade, S. M. B. Costa, Spectroscopic studies of water-soluble porphyrins with protein encapsulated in bis(2-ethylhexyl)sulfosuccinate (AOT) reverse micelles: aggregation versus complexation, *Chem. Eur. J.* 12 (2006) 1046-1057.
- [26] I. E. Borissevitch, T. T. Tominaga, H. Imasato, M. Tabak, Fluorescence and optical absorption study of interaction of two water soluble porphyrins with bovine serum albumin. The role of albumin and porphyrin aggregation, *J. Lumin.* 69 (1996) 65-76.
- [27] C. Z. Huang, Y. F. Li, N. Li, K. A. Li, S. Y. Tong, Spectral characteristics of the aggregation of  $\alpha,\beta,\gamma,\delta$ -tetrakis(p-sulfophenyl)porphyrin in the presence of proteins, *Bull. Chem. Soc. Jpn.* 71 (1998) 1791-1797.
- [28] S. M. Andrade, S. M. B. Costa, Aggregation kinetics of meso-tetrakis(4-sulfonatophenyl) porphine in the presence of proteins: Temperature and ionic strength effects, *J. Fluor.* 12 (2002) 77-82.
- [29] J. Valanciunaite, J. Zerebcova, S. Bagdonas, G. Streckyte, R. Rotomskis, Spectroscopic studies of self-assembled TPPS<sub>4</sub> nanostructures in aqueous solutions: The role of serum albumin and pH, *Lithuanian J. Phys.* 44 (2004) 41-47.
- [30] Y. Fukushima, Interaction of porphyrin derivatives with a beta-sheet structure of a zwitterionic polypeptide in aqueous solution, *Polym. Bull.* 45 (2001) 479-485.
- [31] A. S. R. Koti, N. Periasamy, Self-assembly of template-directed J-aggregates of porphyrin, *Chem. Mater.* 15 (2003) 369-371.
- [32] J. Mosinger, M. Deumie, K. Lang, P. Kubat, D. M. Wagnerova, Supramolecular sensitizer: complexation of meso-tetrakis(4-sulfonatophenyl)porphyrin with 2-hydroxypropyl-cyclodextrins, *J. Photochem. Photobiol., A* 130 (2000) 13-20.
- [33] T. Peters, *All About Albumin: Biochemistry, Genetics, and Medical Applications*, Academic Press, San Diego, 1996.

- [34] D. C. Carter, B. Chang, J. X. Ho, K. Keeling, Z. Krishnasami, Preliminary crystallographic studies of four crystal forms of serum albumin, *Eur. J. Biochem.* 226 (1994) 1049-1052.
- [35] J. R. Lakowicz, *Principles of Fluorescence Spectroscopy*, 3rd ed., Springer, New York, 2006.
- [36] S. Wennmalm, H. Blom, L. Wallerman, R. Rigler, UV-fluorescence correlation spectroscopy of 2-aminopurine, *Biol. Chem.* 382 (2001) 393-397.
- [37] M. Lippitz, W. Erker, H. Decker, K. E. Van Holde, T. Basche, Two-photon excitation microscopy of tryptophan-containing proteins, *Proc. Natl. Acad. Sci. U. S. A.* 99 (2002) 2772-2777.
- [38] J. E. Sanabia, L. S. Goldner, P.-A. Lacaze, M. E. Hawkins, On the feasibility of single-molecule detection of the guanosine-analogue 3-MI, *J. Phys. Chem. B* 108 (2004) 15293-15300.
- [39] H. Zhang, E. S. Yeung, Ultrasensitive native fluorescence detection of proteins with miniaturized polyacrylamide gel electrophoresis by laser side-entry excitation, *Electrophoresis* 27 (2006) 3609-3618.
- [40] Q. Li, T. Ruckstuhl, S. Seeger, Deep-UV laser-based fluorescence lifetime imaging microscopy of single molecules, *J. Phys. Chem. B* 108 (2004) 8324-8329.
- [41] Q. Li, S. Seeger, Label-free detection of single protein molecules using deep UV fluorescence lifetime microscopy, *Anal. Chem.* 78 (2006) 2732-2737.
- [42] S. Seeger, Label-free detection of single native proteins: ultimate sensitivity and convenience, *Chimia* 60 (2006) 854.
- [43] Q. Li, S. Seeger, Label-free detection of protein interactions using deep UV fluorescence lifetime microscopy, *Anal. Biochem.* 367 (2007) 104-110.
- [44] E. Riaplov, Q. Li, S. Seeger, Ultrasensitive staining-free protein detection after PAA gel electrophoresis using deep UV fluorescence, *Protein Pept. Lett.* 14 (2007) 712-715.
- [45] M. Korinek, R. Dedic, A. Molnar, J. Hala, The influence of human serum albumin on the photogeneration of singlet oxygen by meso-tetra(4-sulfonatophenyl)porphyrin. An infrared phosphorescence study, *J. Fluor.* 16 (2006) 355-359.

- [46] S. M. Andrade, T. I. Carvalho, M. I. Viseu, S. M. B. Costa, Conformational changes of beta-lactoglobulin in sodium bis(2-ethylhexyl) sulfosuccinate reverse micelles. A fluorescence and CD study, *Eur. J. Biochem.* 271 (2004) 734-744.
- [47] P. Kubat, K. Lang, P. Anzenbacher, Jr., Modulation of porphyrin binding to serum albumin by pH, *Biochim. Biophys. Acta* 1670 (2004) 40-48.

## Figure captions

Figure 1. Absorption spectra of 2  $\mu\text{M}$  TPPS in the absence and presence of BSA in PBS buffer solution (pH 7.4). The molar ratios of TPPS:BSA (1 $\rightarrow$ 7) is 1:0, 1:0.1, 1:0.3, 1:0.5, 1:1, 1:5, and 1:20, respectively. The insert shows detailed changes for Soret band of TPPS (the spectra for molar ratio 1: 0.75, 1:3 and 1:10 are not shown).

Figure 2. Fitting of absorption spectra of TPPS in the absence and presence of different concentrations of BSA in PBS buffer solution (pH 7.4). [TPPS] = 2  $\mu\text{M}$ , the molar ratios of TPPS:BSA is 1:0, 1:0.3, 1:1, and 1:20, respectively. The open circles are the experimental data. The dotted line indicates absorption of free TPPS, the dashed line is absorption of TPPS-BSA complex. The lower panel shows weighted residuals of each fitting.

Figure 3. The absorption intensity dependence on the BSA concentration for the free TPPS and BSA bound TPPS species at pH 7.4 obtained by Gaussian decomposition of experimental data. [TPPS] = 2  $\mu\text{M}$ .

Figure 4. The fluorescence emission spectra of TPPS in the absence and presence of BSA under excitation at (a) 413 and (b) 422 nm. [TPPS] = 1  $\mu\text{M}$ , the molar ratios of TPPS:BSA (1 $\rightarrow$ 7) is 1:0, 1:0.1, 1:0.5, 1:1, 1:5, 1:10, and 1:20, respectively. The insert shows fluorescence emission dependence on the BSA concentration for the free TPPS and BSA bound TPPS species obtained by fitting experimental data using two distributions.

Figure 5. Fitting of the fluorescence emission spectra of TPPS in PBS buffer solution (pH 7.4) in presence of BSA under excitation at (a) 413 and (b) 422 nm. [TPPS] = 1  $\mu$ M, the molar ratio of TPPS:BSA is 1:0.5. The open circles are the experimental data. The dotted line indicates the fluorescence emission of free TPPS centered at 639 nm, the dashed line is the fluorescence emission of BSA bound TPPS centered at 648 nm. The lower panel shows weighted residuals of each fitting.

Figure 6. Time-resolved fluorescence decay of BSA in the absence and presence of TPPS in PBS buffer solution (pH 7.4) under excitation at 266 nm. BSA concentration was fixed at 1  $\mu$ M, the molar ratios of BSA:TPPS (1 $\rightarrow$ 6) is 1:0, 1:1, 1:2, 1:3, 1:5, and 1:20, respectively. The insert shows the amplitude changes of each lifetime in this titration process.

Figure 7. The fluorescence decay of BSA in the presence of difference of molar ratio TPPS in PBS buffer solution (pH 7.4) excited at 266 nm together with the IRF. The molar ratio of BSA:TPPS is (a) 1:0, (b) 1:3, and (c) 1:20, respectively. The gray lines are the curves to (a) single-, (b) triple-, and (c) double-exponential fluorescence decay. The lower panel shows weighted residuals of each fitting.